Atomic-level physics of grain boundaries in bcc molybdenum

D. Yeşilleten[1] and T. A. Arias[2]

[1]*Department of Physics, Massachusetts Institute of Technology, Cambridge, Massachusetts 02139*
[2]*Laboratory of Atomic and Solid State Physics, Cornell University, Ithaca, New York 14853*
and Research Laboratory of Electronics, Massachusetts Institute of Technology, Cambridge, Massachusetts 02139

We present a systematic trend study of the symmetric tilt grain boundaries about the $\langle 110 \rangle$ axis in molybdenum. Our results show that multiple structural phases, some incorporating vacancies, compete for the boundary ground state. We find that at low external stress vacancies prefer to bind to the boundaries in high concentrations, and moreover, that external stress drives structural phase transitions which correspond to switching the boundaries on and off as pipe-diffusion pathways for vacancies.

I. INTRODUCTION

Molybdenum, with its high melting point and relatively inert chemical nature, is often considered for high-temperature structural applications, but its extreme brittleness limits its usefulness. Quasistatic bicrystal stress-strain experiments[1,2] demonstrate that this brittleness is an intrinsic property of the material and largely unrelated to the presence of impurities. Similar studies observe intergranular fracture at about 1.7 GPa, suggesting that this brittleness arises from weak intergranular cohesion along the grain boundaries.[3] These results also show that impurity concentration does affect intergranular cohesion, but only as a secondary effect. Spallation experiments, on the other hand, show contradictory results. Large-grained (~ 1-mm) samples have been observed to exhibit *trans granular* spall at what the authors of that study consider to be relatively low stresses (~ 2.5 GPa),[4] whereas spallation in fine-grained (~ 5-μm) samples has been observed to be highly *inter granular* in nature and to occur at much higher stresses (15–25 GPa).[5] In an attempt to shed light on this complex situation, we have investigated the microscopic physics of these boundaries. In particular, we have carried out a detailed, atomic-level trend study of the behavior and structure of the low-energy phases of these boundaries and the transitions among these phases.

This study reveals different physics in the interaction of the grain boundaries with vacancies. The traditional mechanisms of interplay between vacancies and grain boundaries include pipe diffusion of vacancies along the boundary,[16–18] and absorption and emission of vacancies during continuous climb of primary or secondary dislocations.[6–10] We find, in addition, that boundary vacancies prefer to collect together at high densities on the boundary plane. Our results also indicate that grain boundaries can either emit or absorb large concentrations of vacancies into the surrounding bulk while undergoing structural phase transitions under applied stress. Our focus in the present study is on the particular system of symmetric tilt boundaries around the $\langle 110 \rangle$ axis in molybdenum, which are known to dominate the recrystallization texture of this material.[3]

II. PROCEDURE

The heavy computational demands of full-blown *ab initio* electronic structure calculations[11] and semiempirical tight-binding models[12–15] restrict their use to the study of relatively small systems and relatively few configurations. In order to understand complex processes such as fracture, dislocation migration, and intergranular cohesion, computationally more feasible empirical potentials must be used. Moriarty has developed such an empirical model based on a multi-ion interatomic potential developed from first-principles generalized pseudopotential theory.[19] The resulting model generalized pseudopotential theory (MGPT) potential, which has been thoroughly described in literature,[19–23] successfully predicts the cohesive, structural, elastic, vibrational, thermal, and melting properties of molybdenum,[21] as well as the ideal shear strength and self-interstitial and vacancy formation energies.[22] We use this potential throughout this work.

We would like to note here that even though the MGPT formalism has been generalized to include local volume changes[23] of potential importance in deformation, defect, and surface calculations, these effects have been shown to be small for bulk defects (~ 0.01-eV vacancy formation energies in bcc metals[22,23]). Accordingly, we here use the simpler form of the MGPT potential as Xu and Moriarty have done in their work on dislocations.[22]

Focusing on the $\langle 110 \rangle$ symmetric tilt boundaries, we consider $\Sigma 3(112)$ and $\Sigma 9(114)$, which are among the lowest in energy, and $\Sigma 3(111)$, $\Sigma 9(221)$, $\Sigma 11(113)$, and $\Sigma 11(332)$ as examples of boundaries with higher energies. To study the physics of these boundaries, which reside in bulk material, we employ periodic boundary conditions as the most natural. To minimize boundary-image interactions, we always maintain at least 17 layers of atoms between boundaries in our supercells.

Determination of the ground state and the low-energy excited state structures in principle requires the exploration of the phase space of all possible configurations, which is an impractical task without taking into account some basic physics. The primary consideration we use to restrict this phase space is that, due to the relatively strong directional bonding in molybdenum and similar bcc metals, the structure of the grain boundaries tends to preserve the *internal* topology of individual grains. Under this restriction, there remain then only three considerations for each boundary: (i) possible addition and removal of atoms to and from the faces of the

grains at the boundary, (ii) the displacement of the grains relative to one another, and (iii) relaxation of the internal atomic coordinates.

For the first consideration, the fact that the interstitial energy in molybdenum (≥ 10 eV) is much larger than the vacancy energy (3 eV) (Ref. 22) indicates that insertion of additional material at the boundary leads to unlikely high interfacial energies. We therefore concentrate only on the *removal* of atoms at the boundary. Direct calculations with the MGPT potential reveal that the most favorable sites for atom removal are in the vicinity of the boundary. It turns out that, because the atoms in the planes adjacent to the boundary plane [indicated by circles in Fig. 1(a)] pack closely together, these sites are the energetically most favorable for vacancy formation.

This leads us to consider the following structural phases for the boundaries in our study: grains joined with the amount of material expected from the *naive* coincident site lattice (CSL) construction ("full-material phase"), and boundaries where we remove atoms from the circled sites in Fig. 1(a), which shows this construction. Below, we find that binding energy per boundary vacancy is higher when vacancies collect together at high density on the boundaries. Therefore we first concentrate on boundaries with high vacancy densities. Because removal of an entire plane of atoms near the boundary is topologically equivalent to the initial full material phase under appropriate relative displacement of the grains, we first focus on the phase where we remove one half plane of atoms from the layer adjacent to the boundary ("vacancy phase").

To determine the ground state of the above two structural phases, we next turn to the second consideration above, the relative shifts of the grains. The displacement-shift complete (DSC) cell, which we explore on a 16×16 sampling grid (which reduces to 4×4 by symmetry), contains all possible unique relative planar shifts of the grains. We then address the third consideration by performing full relaxations of the internal grain coordinates in order to determine the most favorable DSC shift. To complete our search, we then apply a series of external strains which cover the full range of stresses explored below, and we perform full internal relaxations for each strain. This allows us both to identify the ground state and to study the response of the boundary to externally applied strain. We note here that this extensive survey requires force and energy calculations of approximately 400 000 configurations, and would be infeasible to carry out with electronic structure techniques.

To confirm the effectiveness of this survey in identifying ground-state structures, we repeat the above procedure with supercells in which we remove an entire plane of atoms from the boundary. For all six boundaries in our study, our procedure indeed identifies the appropriate shift to recover the initial, topologically equivalent ground state found for the full-material phase before the removal of the plane of atoms.

III. RESULTS

A. Low-energy phases

Our results reveal several general trends in the physics of the $\langle 110 \rangle$ tilt grain boundaries in molybdenum. As a specific
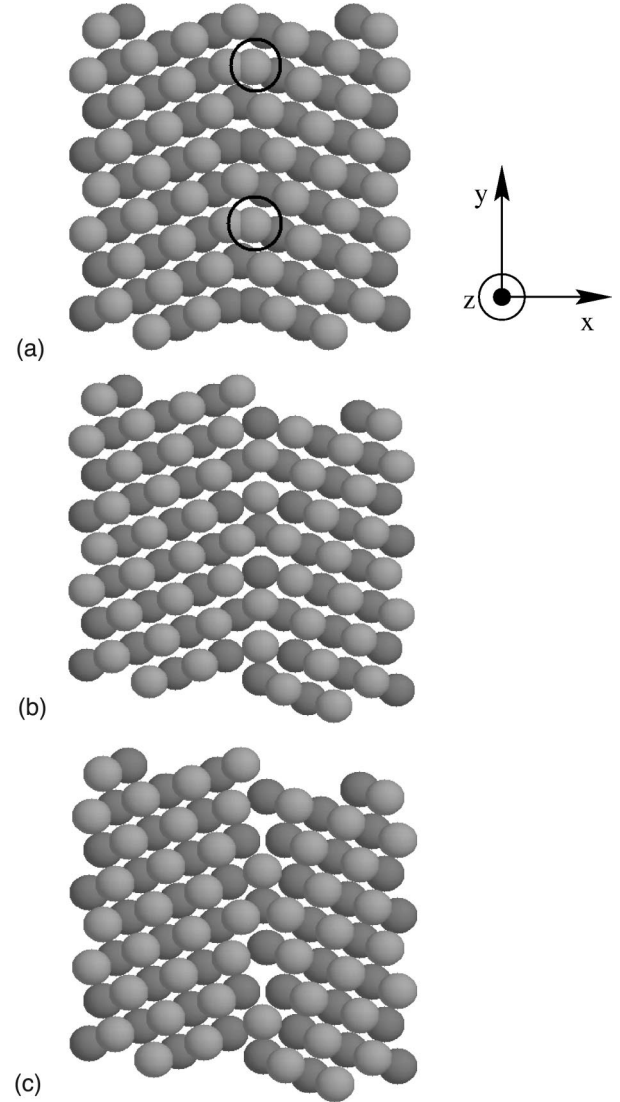

FIG. 1. Structural phases of the $\Sigma 9(114)$ grain boundary: (a) naïve CSL boundary, (b) relaxed full-material boundary, (c) relaxed vacancy phase boundary. (To aid visualization, atoms from the two cubic sublattices are colored separately, light and dark.)

example, consider the $\Sigma 9(114)$ boundary, which Fig. 1 shows. Figure 1(a) shows the naive CSL construction of the full-material phase, whose ground state as identified through our procedure, appears in Fig. 1(b). We find that this phase lowers its energy through both a perpendicular expansion of the boundary and intergranular shifts parallel to the boundary, both of which tend to increase the local volume for the closely packed atoms near the boundary plane, restoring them to a more bulklike environment.

Table I shows that the outward expansion is a general trend among all grain boundaries in our study and that shifts occur along the boundary in the direction perpendicular to the tilt axis (y direction, Fig. 1) to allow for a more bulklike local environment. We find no significant shifts along the tilt axis (z direction, Fig. 1) for this phase of any of the boundaries. The next column of the table gives the mechanical compliance ($1/k$) of each boundary, where k is determined

TABLE I. Full-material phase: energies ($\mathcal{U}_o$), perpendicular expansions (Δx), shifts (Δy and Δz) relative to the CSL construction, compliances [$\Delta(1/k)$], and anharmonic coefficients (Δa) relative to bulk. Coordinates are as defined in Fig. 1.

Boundary	$\mathcal{U}_o$ [mJ/m^2]	Δx [Å]	Δy [Å]	Δz [Å]	$\Delta(1/k)$ [mJ/m^2] $\times 10^{-20}$	$\Delta(a)$ [m^6/mJ^2] $\times 10^{-30}$
$\Sigma 3(112)$	610	0.1	0.3	0.0	900	1
$\Sigma 3(111)$	2020	0.5	0.3	0.0	4770	-306
$\Sigma 9(114)$	1730	0.5	0.1	0.0	3410	-27
$\Sigma 9(221)$	2180	0.4	0.1	0.0	100	15
$\Sigma 11(113)$	1740	0.5	0.2	0.0	1460	-15
$\Sigma 11(332)$	2160	0.4	0.5	0.0	580	-29

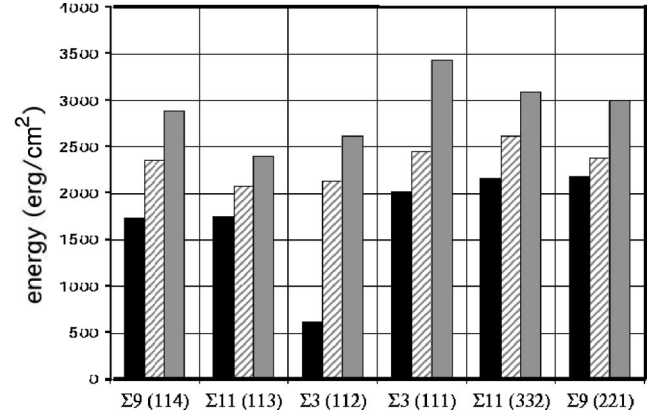

FIG. 2. Energetics of grain boundary phases: full-material phase (black bars), vacancy phase (hatched bars), bulk-vacancy phase (gray bars).

from the quadratic response of the energy per unit area per boundary as the cell expands. Finally, the last column of the table lists $a \equiv \alpha/k^3$, where α captures any nonquadratic behavior in the energy expression

$$\mathcal{U} = \mathcal{U}_o + \tfrac{1}{2} k(x - \Delta x)^2 + \tfrac{1}{6} \alpha(x - \Delta x)^3 + \cdots, \quad (1)$$

where x is the expansion of the cell, and Δx and $\mathcal{U}_o$ are the relaxed perpendicular expansion and boundary energy given in the table, respectively. The table lists the difference between $1/k$ and a for the boundary and for the same cell filled with bulk, as it is these differences which define the response of the boundary, *independent* of the bulk content of the cell.

Turning now to the vacancy phase, Fig. 1(c) shows the results of our ground-state search for the $\Sigma 9(114)$ boundary as formed by removing the circled atoms from Fig. 1(a). We again find grain shifting as well as local internal relaxations to create more bulklike local atomic environments, as Table II summarizes. The perpendicular shift is always *inward* compared to the ground state of the full-material phase, so as to close the material void associated with the vacancies. Finally, we frequently find for the vacancy phase, even for the highly stable $\Sigma 3$'s, parallel shifts relative to the full-material phase which produce more natural bonding arrangements for the boundary to accommodate the vacancies. This tendency for accommodation is so strong as to induce the only shift

TABLE II. Vacancy phase: energies ($\mathcal{U}_o$), perpendicular expansions (Δx), shifts (Δy and Δz) relative to the CSL construction, compliances [$\Delta(1/k)$], and anharmonic coefficients (Δa) relative to bulk. Coordinates are as defined in Fig. 1.

Boundary	$\mathcal{U}_o$ [mJ/m^2]	Δx [Å]	Δy [Å]	Δz [Å]	$\Delta(1/k)$ [mJ/m^2] $\times 10^{-20}$	$\Delta(a)$ [m^6/mJ^2] $\times 10^{-30}$
$\Sigma 3(112)$	2130	-0.1	0.4	0.0	3030	-24
$\Sigma 3(111)$	2450	0.1	0.3	0.0	1440	-62
$\Sigma 9(114)$	2360	0.3	0.1	0.0	7250	11
$\Sigma 9(221)$	2380	0.3	0.9	0.0	2210	17
$\Sigma 11(113)$	2070	0.3	0.8	0.0	2370	28
$\Sigma 11(332)$	2590	0.2	0.4	0.8	2400	26

along the tilt axis we observe in this study, for the vacancy phase of the $\Sigma 11(332)$ boundary.

Figure 2 compares the ground-state boundary energies of the various phases. In all cases, we find the full-material phase (black bars) to be lower in energy than the vacancy phase (hatched bars), although often not by far. As in the experimental case, MGPT predicts the lowest ground-state interfacial energy to be for the naturally occurring twin $\Sigma 3$ (112) boundary.[3] Moreover, apart from this twin, all remaining ground-state boundary energies are fairly constant (within 25%), as also found in experiment [within 30% (Ref. 3)].

Figure 2 presents another relevant comparison. To transform physically into the full-material phase, the vacancy phase must first expel its vacancies into the surrounding bulk material. Thus, when considering transitions, the relevant comparison is between the vacancy phase and a third phase, which consists of the full-material phase plus the corresponding number of vacancies in the surrounding bulk material ("bulk-vacancy phase"). To describe the enthalpies of isolated vacancies in bulk under external stresses applied in the direction corresponding to the orientation of each boundary, we repeat the procedure from Sec. II with the same supercells, but filled with bulk material and a single vacancy. Table III summarizes the results. The resulting energies may then be added to the full-material phase to produce the energy of the bulk-vacancy phase (gray bars in Fig. 2). Figure 2 shows that, although creation of vacancies on the boundary always increases the boundary energy, the energy for creating the corresponding number of vacancies in the bulk is always higher. Our results therefore are consistent with the fact that the boundaries act as reservoirs for vacancies, as occurs during pipe diffusion.

To verify, as mentioned above in Sec. II, that boundary vacancies indeed prefer to cluster together, we have also considered boundaries with nearly isolated vacancies within our supercell approach. Table IV presents energy, displacement, compliance, and anharmonic results for boundaries from supercells with low vacancy densities ("dilute-vacancy phase"). In these calculations, the vacancy concentration

TABLE III. Isolated vacancy enthalpy information for each boundary orientation. Results are expressed for the number of vacancies per unit area of the corresponding boundary-vacancy phase. Lattice expansion Δx, compliance $\Delta(1/k)$, and anharmonic Δa information are for longitudinal strain perpendicular to the boundary plane.

Boundary	$\mathcal{U}_o$ [mJ/m^2]	Δx [Å]	$\Delta(1/k)$ [mJ/m^2] $\times 10^{-20}$	$\Delta(a)$ [m^6/mJ^2] $\times 10^{-30}$
$\Sigma 3(112)$	130	-0.003	1050	-1
$\Sigma 3(111)$	100	-0.002	870	-117
$\Sigma 9(114)$	80	0.003	500	-32
$\Sigma 9(221)$	60	-0.001	470	0
$\Sigma 11(113)$	50	-0.001	130	-5
$\Sigma 11(332)$	60	-0.005	180	-39

(3.3%) is $\frac{1}{15}$ th that of the vacancy phase. Table V compares the boundary-vacancy binding energies for the vacancy and dilute-vacancy phases. As the larger binding energies reflect, the concentrated phase (*vacancy phase*) is more stable. This added stability appears to arise from the structural relaxation through parallel shifting of the grains, which the high density of vacancies makes possible. Finally, we observe that in the extreme case of the $\Sigma 11$ boundaries, vacancies do not even bind to the boundary at low concentrations.

B. Phase transitions

Three trends which the preceding results exhibit can be expected from general, material-independent considerations: (i) that the boundaries present preferred binding sites for vacancies because they disrupt the bulk bond order, (ii) that boundary vacancies prefer to collect into the high-density vacancy phases because of the additional relaxation, which parallel shifting of the grains affords, and (iii) that the binding of vacancies to the boundary reduces the intergranular spacing because this restores more bulklike interatomic separations. These phenomena open the intriguing possibility that the application of tensile stress normal to grain boundaries in

TABLE IV. Dilute-vacancy phase: energies ($\mathcal{U}_o$), perpendicular expansions (Δx), shifts (Δy and Δz) relative to the CSL construction, compliances [$\Delta(1/k)$] and anharmonic coefficients (Δa) relative to bulk. Coordinates are as defined in Fig. 1.

Boundary	$\mathcal{U}_o$ [mJ/m^2]	Δx [Å]	Δy [Å]	Δz [Å]	$\Delta(1/k)$ [mJ/m^2] $\times 10^{-20}$	$\Delta(a)$ [m^6/mJ^2] $\times 10^{-30}$
$\Sigma 3(112)$	720	0.1	0.3	0.0	950	-22
$\Sigma 3(111)$	2076	0.5	0.3	0.0	2060	2
$\Sigma 9(114)$	2360	0.4	0.1	0.0	3520	-10
$\Sigma 9(221)$	2200	0.3	0.1	0.0	260	-69
$\Sigma 11(113)$	1900	0.5	0.2	0.0	1900	-3
$\Sigma 11(332)$	2250	0.4	0.5	0.0	990	-125

TABLE V. Boundary-vacancy binding energies at high and low densities. (The $\Sigma 11$ boundaries do not bind vacancies at low concentrations.)

Boundary	Binding energy per vacancy at high density [eV]	Binding energy per vacancy at low density [eV]
$\Sigma 3(112)$	0.7	0.6
$\Sigma 3(111)$	2.1	1.1
$\Sigma 9(114)$	1.4	0.7
$\Sigma 9(221)$	2.3	2.0
$\Sigma 11(113)$	1.4	-7.1
$\Sigma 11(332)$	1.4	-1.7

bcc metals generally drives transitions among these various structural phases, thereby providing new forms of boundary-vacancy interaction.

To explore this possibility, we consider the thermodynamic potential which is minimized under fixed external stress, the enthalpy. As a function of applied perpendicular stress σ, the enthalpy of a grain-boundary structure relative to bulk is

$$\Delta\mathcal{H} = \Delta\mathcal{U}_o - \Delta x\,\sigma - \tfrac{1}{2}\,\Delta(1/k)\sigma^2 + \tfrac{1}{6}\,\Delta a\,\sigma^3 + \mathcal{O}(\sigma^4). \tag{2}$$

Here $\Delta\mathcal{U}_o$ is the difference in the ground-state energy per unit area, Δx is the difference in preferred perpendicular intergranular separation, $\Delta(1/k)$ is the difference in compliance, and $\Delta a \equiv \Delta(\alpha/k^3)$ captures the difference in the nonquadratic behavior of the energies. Each of these materials parameters appears for each relevant phase in Tables I–IV.

As an example, Fig. 3 shows the behavior of the enthalpy, relative to bulk, of the naturally occurring $\Sigma 3(112)$ boundary in its full-material, vacancy, and bulk-vacancy phases. Three first-order phase transitions (enthalpy crossings) are evident in the figure. At zero stress, as observed above, the full-material phase is the ground state of the boundary, and moreover, in the presence of vacancies, the vacancy phase has lower energy than the bulk-vacancy phase, indicating that vacancies prefer the boundary over the bulk. However, at an applied stress of about 18 GPa (σ_c^{emit}) within MGPT, the $\Sigma 3(112)$ boundary system undergoes a first-order phase transition in which the vacancy phase is no longer preferred, and the boundary ejects its vacancies into the surrounding bulk material. A second transition occurs near 25 GPa (σ_c^{bulk}), at which point the bulk-vacancy phase becomes lower in enthalpy than the bulk material phase. This corresponds to the *spontaneous* formation of vacancies in bulk, indicating breakdown of the bulk material. The third transition occurs near 30 GPa (σ_c^{gb}). Were this transition accessible before the breakdown of the bulk material, it would correspond to spontaneous formation of boundary vacancies.

It is important to note that many modes of failure in addition to spontaneous formation of vacancies are accessible to the bulk and boundaries. The transition stresses which we
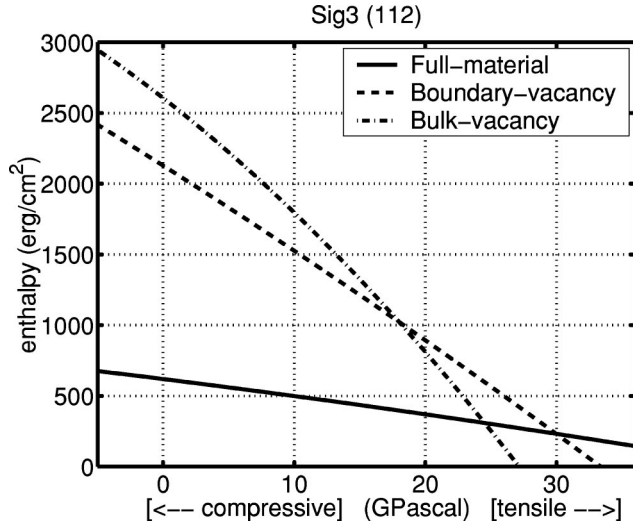
FIG. 3. Enthalpies of $\Sigma 3(112)$ boundary as a function external stress for all three phases.

report for breakdown, therefore, can be regarded only as upper bounds when making comparisons to experimental results.

Table VI presents the stresses for the above three transitions for all boundaries in our study. In all cases, the emission stress is accessible before breakdown of the bulk material through spontaneous formation of vacancies. Moreover, except the for the outlying behaviors of the $\Sigma 9(221)$ and $\Sigma 11(332)$ boundaries, vacancies always first form spontaneously in the bulk before they do so on the boundaries.

To verify that these results are not artifacts of the high-density vacancy phase, we repeat the above enthalpy analysis for boundaries with low densities of vacancies using the data of Table IV. As Table VII summarizes, we again observe the same transitions. The $\Sigma 11$ boundaries do not bind vacancies at low concentrations (Table V), and therefore the transition stresses for the emission of vacancies for these boundaries are not physically relevant. For the lower Σ boundaries [except the $\Sigma 9(221)$ boundary, which again exhibits an outlying behavior], diluting the vacancy concentration reduces the critical emission stress at which the boundaries emit boundary vacancies into the bulk (σ_c^{emit}), thus making this transition more accessible.

TABLE VI. Critical stresses for the phase transitions discussed in the text: emission of vacancies from the boundary into the bulk (σ_c^{emit}), breakdown of the bulk through spontaneous formation of vacancies (σ_c^{bulk}), spontaneous formation of vacancies at the boundary (σ_c^{gb}).

Boundary	σ_c^{emit} [GPa]	σ_c^{bulk} [GPa]	σ_c^{gb} [GPa]
$\Sigma 3(112)$	18	25	30
$\Sigma 3(111)$	15	20	66
$\Sigma 9(114)$	19	21	42
$\Sigma 9(221)$	38	24	10
$\Sigma 11(113)$	21	27	45
$\Sigma 11(332)$	31	27	22

TABLE VII. Critical stresses for the same transitions as in Table VI, but at 3.3% vacancy concentration.

Boundary	σ_c^{emit} [GPa]	σ_c^{bulk} [GPa]	σ_c^{gb} [GPa]
$\Sigma 3(112)$	17	25	29
$\Sigma 3(111)$	11	20	40
$\Sigma 9(114)$	9	21	61
$\Sigma 9(221)$	26	24	6
$\Sigma 11(113)$	56	27	81
$\Sigma 11(332)$	37	27	31

Finally, as we expect from the fact that boundary vacancies are more stable in high concentrations, the stress required to induce formation of vacancies on the boundaries (σ_c^{gb}) at low densities is generally greater than for the high-density vacancy phase. As a last consistency check on our analysis, we note that the stress for breakdown of the bulk through the spontaneous formation of vacancies (σ_c^{bulk}), as a characteristic of the perfect crystal and not the boundary, remains essentially unchanged between the two independent sets of calculations for low and high boundary vacancy concentrations.

IV. CONCLUSIONS

We expect that the following conclusions likely hold generally for the interactions among vacancies and tilt grain boundaries: (i) consistent with the traditional view of grain boundaries as diffusion pathways, vacancies prefer the boundaries over the bulk at low stresses, (ii) boundary vacancies prefer to collect into high-density vacancy phases, (iii) application of sufficient tensile stress to a boundary induces a structural phase transition which drives the vacancies from the boundaries into the bulk, thereby shutting off pipe diffusion along the boundary. The last of these conclusions in particular may have important implications for crack growth through pipe-diffusion assisted void growth and void formation at grain boundaries.

Finally, in terms of precise *quantitative* predictions of the critical stresses characterizing these phenomena, it is important to bear in mind that the particular interatomic potential which we have employed (MGPT), although one of the most reliable for Mo, is known to exaggerate energy scales for complex structures.[24] We therefore expect to find these same transitions, but most likely at lower stresses, when studied either experimentally or *ab initio*.

[1] H. Kurishita, A. Oishi, H. Kubo, and H. Yoshinaga, J. Jpn. Inst. Met. **47**, 539 (1983); Trans. Jpn. Inst. Met. **26**, 332 (1985).

[2] T. Tanaka, S. Tsurekawa, H. Nakashima, and H. Yoshinaga, J. Jpn. Inst. Met. **58**, 382 (1994).

[3] S. Tsurekawa, T. Tanaka, and H. Yoshinaga, Mater. Sci. Eng., A **176**, 341 (1994).

[4] V.K. Golubev, S.A. Novikov, Yu.S. Sobolev, and N.A. Yukina, Strength Mater. **17**, 515 (1985).

[5] L.E. Murr, J. Appl. Phys. **47**, 1364 (1976).

[6] R.W. Balluffi, Phys. Status Solidi **31**, 443 (1969).

[7] R. W. Balluffi and A.V. Granato, in *Dislocations in Solids*, edited by F.R.N. Nabarro (North-Holland, Amsterdam, 1979) Vol. 4, p. 1.

[8] J. P. Hirth and J. Lothe, in *Theory of Dislocations*, 2nd ed. (Wiley, New York, 1982).

[9] A. P. Sutton and R.W. Balluffi, *Interfaces in Crystalline Materials* (Clarendon, Oxford, 1995), p. 606.

[10] A. P. Sutton and R.W. Balluffi, *Interfaces in Crystalline Materials* (Ref. 9), p. 614.

[11] M.C. Payne *et al.*, Rev. Mod. Phys. **64**, 1045 (1992).

[12] A.E. Carlsson, Phys. Rev. B **44**, 6590 (1991).

[13] D.G. Pettifor, Phys. Rev. Lett. **63**, 2480 (1989); M. Aoki, *ibid.* **71**, 3842 (1993).

[14] S.M. Foiles, Phys. Rev. B **48**, 4287 (1993).

[15] W. Xu and J.B. Adams, Surf. Sci. **301**, 371 (1994).

[16] K.M. Miller, K.W. Ingle, and A.G. Crocker, Acta Metall. **29**, 1599 (1981).

[17] K.W. Ingle and A.G. Crocker, J. Nucl. Mater. **69-70**, 667 (1978).

[18] K.W. Ingle and A.G. Crocker, Philos. Mag. **37**, 297 (1978).

[19] J.A. Moriarty, Phys. Rev. B **38**, 3199 (1988).

[20] J.A. Moriarty, Phys. Rev. B **42**, 1609 (1990).

[21] J.A. Moriarty, Phys. Rev. B **49**, 12 431 (1994).

[22] W. Xu and J.A. Moriarty, Phys. Rev. B **54**, 6941 (1996).

[23] J.A. Moriarity and R. Phillips, Phys. Rev. Lett. **66**, 3036 (1991).

[24] S. Ismail-Beigi and T.A. Arias, Phys. Rev. Lett. **84**, 1499 (2000).